

Accepted Manuscript

Numerical simulations with the P-Hydroslog model to predict phosphorus removal by steel slag filters

Dominique Claveau-Mallet, Benoît Courcelles, Philippe Pasquier, Yves Comeau



PII: S0043-1354(17)30787-X

DOI: [10.1016/j.watres.2017.09.032](https://doi.org/10.1016/j.watres.2017.09.032)

Reference: WR 13226

To appear in: *Water Research*

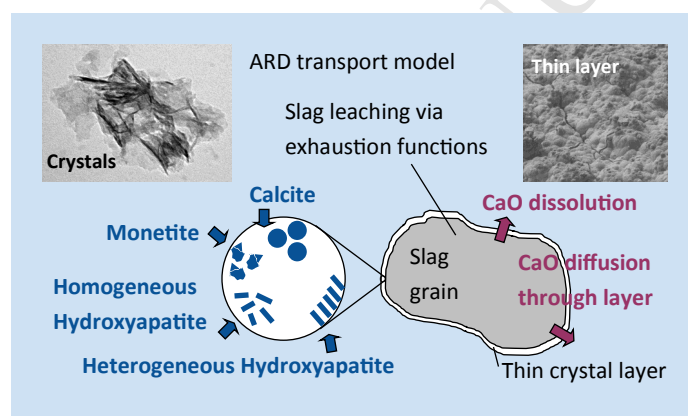
Received Date: 9 March 2017

Revised Date: 8 September 2017

Accepted Date: 17 September 2017

Please cite this article as: Claveau-Mallet, D., Courcelles, Benoît., Pasquier, P., Comeau, Y., Numerical simulations with the P-Hydroslog model to predict phosphorus removal by steel slag filters, *Water Research* (2017), doi: 10.1016/j.watres.2017.09.032.

This is a PDF file of an unedited manuscript that has been accepted for publication. As a service to our customers we are providing this early version of the manuscript. The manuscript will undergo copyediting, typesetting, and review of the resulting proof before it is published in its final form. Please note that during the production process errors may be discovered which could affect the content, and all legal disclaimers that apply to the journal pertain.



Numerical simulations with the P-Hydroslag model to predict phosphorus removal by steel slag filters

By Dominique Claveau-Mallet*, Benoît Courcelles, Philippe Pasquier, and Yves Comeau

Department of Civil, Geological and Mining Engineering, Polytechnique Montreal, Montreal, Quebec, Canada, H3C 3A7

* corresponding author: Dominique.claveau-mallet@polymtl.ca

ABSTRACT

The first version of the P-Hydroslag model for numerical simulations of steel slag filters is presented. This model main original feature is the implementation of slag exhaustion behavior, crystal growth and crystal size effect on crystal solubility, and crystal accumulation effect on slag dissolution. The model includes four mineral phases: calcite, monetite, homogeneous hydroxyapatite (constant size and solubility) and heterogeneous hydroxyapatite (increasing size and decreasing solubility). In the proposed model, slag behavior is represented by CaO dissolution kinetic rate and exhaustion equations; while slag dissolution is limited by a diffusion rate through a crystal layer. An experimental test for measurement of exhaustion equations is provided. The model was calibrated with an experimental program made of three phases. Firstly, batch tests with 300 g slag sample in synthetic solutions were conducted for the determination of exhaustion equation. Secondly, a slag filter column test fed with synthetic solution was run for 623 days, divided into 9 cells and sampled at the end of the experiment. Finally, the column was dismantled, sampled and analyzed with XRD, TEM and SEM. Experimental column curves for pH, oPO_4 , Ca and inorganic carbon were well predicted by the model. Crystal sizes measured by XRD and TEM validated the hypothesis for homogeneous precipitation while SEM observations validated the thin crystal layer hypothesis. A preliminary validation of the model resulted in successful predictions of a steel slag filter longevity fed with real wastewater.

KEYWORDS

slag, phosphorus, wastewater treatment modelling, PHREEQC, hydroxyapatite, calcite, precipitation

26 ABBREVIATIONS

27	Symbol	Description
28	<u>General abbreviations</u>	
29	BOF	Basic oxygen furnace
30	CW	Constructed wetlands
31	EAF	Electric arc furnace
32	HRT _v	Hydraulic retention time of voids
33	MONtoHAP	Transformation of MON into HAP
34	o-PO ₄	Ortho-phosphates
35	SEM	Scanning electron microscope
36	TEM	Transmission electron microscope
37	TIC	Total inorganic carbon
38	WW	Wastewater
39	XRD	X-Ray diffraction
40	<u>Abbreviations for mineral phases</u>	
41	CAL	Calcite CaCO ₃
42	HAP	Hydroxyapatite Ca ₅ OH(PO ₄) ₃
43	HAP_HO	Primary hydroxyapatite via homogeneous precipitation Ca ₅ OH(PO ₄) ₃
44	HAP_HE	Primary hydroxyapatite via heterogeneous precipitation Ca ₅ OH(PO ₄) ₃
45	HAP2	Secondary hydroxyapatite via monetite transformation Ca ₄ OH ₂ (PO ₄) ₂
46	MON	Monetite CaHPO ₄
47	Symbol	Description Units (value)
48	<u>Constants</u>	
49	a_{HAP_0}	HAP crystal size in homogeneous precipitation [m]
50	B_1 and B_2	Regression coefficients in k_{diss} exhaustion function
51	D^*	Dispersivity (transport model) [cm]
52	D_n	Exchange factor between effective and immobile porosity (transport model) [s ⁻¹]
53	k_{CAL}	CAL precipitation constant [mol CAL/s m ² slag]
54	k_{HAP}	HAP precipitation constant [mol HAP/s m ² slag]
55	k_{MON}	MON precipitation constant [mol MON/s m ² slag]

56	$k_{MONtoHAP}$	MONtoHAP precipitation constant [M HAP ² /(M MON s)]	
57	K_{spCAL}	Solubility product for CAL	[M ²]
58	K_{spHAP_bulk}	Bulk solubility product for HAP (Stumm and Morgan, 1996)	[10 ⁻⁵⁷ M ⁹]
59	K_{spHAP_HO}	Solubility product for HAP_HO	[M ⁹]
60	K_{spMON}	Solubility product for MON	[M ²]
61	L_{HAP}	L/D ratio for columnar HAP crystals	[-]
62	mv_{exp}	Slag mass to water volume ratio in a batch test	[g/mL]
63	MW_{HAP}	HAP Molecular weight	[502 g/mol]
64	n	Total porosity in the slag filter	[-]
65	n_e	Effective porosity in the slag filter	[-]
66	n_{im}	Immobile porosity in the slag filter	[-]
67	P_1, P_2, P_3 and P_4	Regression coefficients in pH_{sat} exhaustion function	
68	R	Ideal gas constant	[8.31 J mol ⁻¹ K ⁻¹]
69	S	Slag specific surface	[m ² /m ³]
70	se_{HAP_0}	initial HAP seeds concentration	[seeds/L]
71	SI_c	Critical saturation index between HAP_HE and HAP_HO	[-]
72	T	Temperature	[K]
73	γ	HAP mean free surface energy (Stumm and Morgan, 1996)	[87 mJ/m ³]
74	ρ_{barr}	Crystal concentration in the crystal barrier	[g crystal/m ³]
75	ρ_{HAP}	HAP crystal density (Klein et al., 2002)	[3 600 000 g/m ³]
76	ρ_{slag}	Slag grain density	[3.8 g/mL]
77	<u>Rates, functions and variables</u>		
78	a_{HAP}	Mean HAP crystal size	[m]
79	b_{im}	Moles of an element in immobile porosity (transport model)	[mol]
80	C	Total dissolved concentration for an element (transport model)	[mol/kgw]
81	C_e	C in effective porosity (transport model)	[mol/kgw]
82	C_{im}	C in immobile porosity (transport model)	[mol/kgw]
83	$CaOl_{BATH}$	Leached CaO in a acid bath	[mol/g]
84	CaO_{KTEST}	Leached CaO in a batch test	[mol/g]
85	$CaOl_{TOT}$	Cumulative leached CaO in a batch test	[mol/g]
86	D_{barr}	Diffusion coefficient in the crystal barrier	[m ² /s]

87	d_{barr}	Thickness of the crystal barrier	[m]
88	k_{diss}	Slag dissolution constant	[mol CaO/m ² slag]
89	K_{spHAP_HE}	Solubility product for HAP_HE	[M ⁹]
90	pH_{sat}	Saturation pH in the slag filter	[-]
91	q	Concentration in the solid phase for an element (transport model)	[mol/kgw]
92	r_{CAL}	CAL precipitation rate	[M CAL/s]
93	r_{diff}	CaO diffusion rate through crystal barrier	[M CaO/s]
94	r_{diss}	Slag dissolution rate	[M CaO/s]
95	r_{HAP_HE}	Primary heterogeneous HAP precipitation rate	[M HAP/s]
96	r_{HAP_HO}	Primary homogenous HAP precipitation rate	[M HAP/s]
97	r_{MON}	MON precipitation rate	[M MON/s]
98	$r_{MONtoHAP}$	Secondary HAP precipitation rate	[M HAP ² /s]
99	S_{HAP}	HAP molar specific surface	[m ² /mol]
100	se_{HAP}	HAP seeds concentration	[units/L]
101	SF_{diff}	Step function in diffusion rate	[-]
102	SF_{diss}	Step function in dissolution rate	[-]
103	SF_{HAP_HE}	Step function in HAP_HE rate	[-]
104	SF_{HAP_HO}	Step function in HAP_HO rate	[-]
105	SI_{HAP_HE}	Saturation index for HAP_HE	[-]
106	SI_{HAP_HO}	Saturation index for HAP_HO	[-]
107	t	Time (transport model)	[s]
108	v	Pore water flow velocity (transport model)	[m/s]
109	x	1D distance (transport model)	[m]
110	X_{CaO}	Total leached CaO in the slag filter	[M]

111 112 1 Introduction

113 Steel slag filters are an effective and passive technology for phosphorus removal from wastewater,
 114 allowing typical municipal effluent o-PO₄ concentration below 0.5 mg P/L (Kõiv et al., 2016). Design tools
 115 for slag filters are not yet developed and full scale slag filters cannot be implemented without expensive

pilot tests. The main issue related to steel slag filter operation relies on filter exhaustion and a relatively rapid drop of removal efficiency (Chazarenc et al., 2008). A tool providing the effect of influent composition and operational conditions (type and size of slag, influent flowrate, filter geometry) on slag filter effluent o-PO_4 concentration and longevity would facilitate the design of these systems. This paper presents the P-Hydroslog model, a new model adapted for steel slag filter simulations considering influent composition and void hydraulic retention time (HRT_v) while being compatible with accepted physicochemical modeling frameworks (Lizarralde et al., 2015; Mbamba, Batstone et al., 2015; Mbamba, Tait et al., 2015).

Sorption isotherms were largely proposed as a design tool for steel slag filters (Vohla et al., 2011), but this method does not consider void precipitation and long-term changes in the material properties, explaining why isotherms could not yet predict correctly full-scale behavior. The $k\text{-C}^*$ model traditionally used for constructed wetlands (Kadlec and Wallace, 2009) successfully predicted steel slag filter performance (Barca et al., 2013). This method may be suitable for design, but it cannot estimate the lifetime of the filter. A general correlation between material CaO content and P retention capacity based on several studies was proposed by Vohla et al. (2011), highlighting the importance of CaO dissolution in retention mechanisms. Such a design tool, however, does not consider important aspects as CaO availability, HRT_v or influent composition, leading to a prediction uncertainty that is not acceptable for design purpose. Finally, a predictive model based on several material properties, HRT_v and inlet P concentration was proposed (Penn et al., 2016). This model's strengths were to consider both Fe-Al and Ca based materials, propose an empiric relationship between material buffering capacity and P retention capacity, and predict P retention for both lab-scale and pilot-scale systems. This model, however, did not include direct measurement of kinetic rates, and would not be compatible with general physicochemical modeling frameworks in wastewater treatment.

Two previous modeling studies were published in the recent years. The first study (Claveau-Mallet et al., 2012) qualitatively described concepts forming the basis of the model, including slag dissolution, hydroxyapatite precipitation, crystal formation and accumulation in voids, and effect of velocity on crystal accumulation. In the second study (Claveau-Mallet et al., 2014), concepts were translated into a prototype model including mathematical equations for precipitation and slag exhaustion, and a proposition of laboratory protocol for slag characterization was presented. Numerical simulations of a slag filter were performed on the base of this prototype model without experimental program for calibration. Results were realistic but overestimated the filter longevity. Predictions from the 2014 prototype model were compared to full-scale real data in a recent study (Köiv et al., 2016) in which longevity was overestimated.

In this paper, the first full version of the P-Hydroslag (standing for Phosphorus-hydroxyapatite-slag) model is presented. The P-Hydroslag model is similar to the 2014 prototype model, with additional features for diffusion barrier and crystal growth, a refined characterization of exhaustion equations, and a complete model equation matrix. The objectives were to calibrate the P-Hydroslag model with experimental data and evaluate the validity and realism of the model.

2 Material and Methods

2.1 Slag media

5-10 mm electric arc furnace steel slag produced by Arcelor Mittal and provided by Minéraux Harsco (Contrecoeur, Canada) was used (33% Fe_2O_3 , 30% CaO , 16% SiO_2 , 12% MgO , 6% Al_2O_3 and 3% other metallic oxides). Its density (3.8) and specific surface ($0.308 \text{ m}^2/\text{g}$) were determined according to the ASTM C127-04 standard (ASTM, 2004) and the Brunauer, Emmet and Teller method (Lowell et al., 2004). Slag from the same source was previously studied by the authors' research team for wastewater

treatment applications (Claveau-Mallet et al., 2015; Claveau-Mallet et al., 2013; Kõiv et al., 2016) or modeling studies (Claveau-Mallet et al., 2014; Claveau-Mallet et al., 2012).

2.2 Column test

A vertical filter column filled with slag was fed from its base with a synthetic wastewater in a saturated mode for a total duration of 623 days at approximately 25°C. The column size was 159 cm in length and 10 cm in internal diameter. The synthetic wastewater solution consisted of K_2HPO_4 , KH_2PO_4 , $NaHCO_3$ and $CaCl_2$ in tap water. The influent mean composition was pH of 7.80 ± 0.2 , ortho-phosphates ($o-PO_4$) of 8.9 ± 2.0 mg P/L, total inorganic carbon (TIC) of 22 ± 2 mg C/L, Ca of 54 ± 14 mg/L and alkalinity of 102 ± 3 mg $CaCO_3$ /L. The influent flowrate was 6.9 ± 1.0 mL/min for the first 517 days and 3.4 ± 0.5 mL/min for the remaining 106 days of operation.

The column was divided into 11 virtual cells for the filling step, identified #0 to #10, with #0 at bottom (inlet) and #10 at top (outlet). Cells #1 to #9 were 15 cm long and had a sampling hole in the middle. Cells #0 and #10 were 7.5 cm long and had no sampling hole to provide a slag transition zone between the inlet/outlet tubing and sampling zones. While filling the column, two 300 g slag samples were taken from each cell using a standard sampling procedure for aggregate materials (ASTM C702, 2011). Slag samples were used in batch kinetic tests (presented in section 2.3). The total slag mass in the column was 24.24 kg, resulting in a 49.2% porosity.

The feeding barrel, column effluent and cells were sampled and analyzed periodically for pH, $o-PO_4$, filtered Ca, settled TIC, total P and alkalinity, using standard procedures (APHA, AWWA and WEF, 2012). A maximum of 3 cells were sampled in the same day to minimize perturbation, resulting in a monthly sampling frequency for each cell (twice a month in the second feeding phase). The feeding barrel and effluent column sampling frequency was weekly for pH and once or twice a month for the other parameters. Tracer tests were conducted after 12, 69, 82, 107, 187, 271, 376 and 558 days. Rhodamine

at a concentration of 20 mg/L was used as a tracer and measured in the effluent using spectrofluorometry.

At the end of operation, feeding was stopped and the column was kept saturated for 6 days before dismantling. Upon dismantling, pore water was first sampled and analyzed, then the column was cut into 4 sections to ensure efficient solids sampling. For each cell, three samples were taken: first, several slag particles sampled before doing any major disturbance of the slag media (for scanning electron microscope (SEM) analysis). Second, slag was washed with water in a large pan and precipitates were sampled by sedimentation (for X-ray diffraction (XRD) and transmission electron microscope (TEM) analyses). Finally, a 300 g of washed slag sample was taken for kinetic tests (described in section 2.3). Precipitates were air-dried for 3 days, sieved at mesh 60 and cleaned from slag dust with a strong magnet. Precipitates were analyzed with XRD using a Philipps X'Pert diffractometer operated at 50 kV and 40 mA, using the Bragg-Brentano geometry and a CuK_α radiation. The Scherrer equation (Cullity, 2001) was used to estimate mean crystal sizes from diffractograms, using the $\sim 26.1^\circ$ peak for hydroxyapatite (HAP) and $\sim 29.4^\circ$ peak for calcite (CAL). Precipitates of cells 1, 2, 3 and 8 were analyzed using TEM with the bright field imaging technique (Jeol JEM-2100f field emission gun microscope, 200 kV). Before TEM analysis, samples were prepared with a 30-s ultrasound bath in methanol, and placed on a copper grid covered with Formvar lightly coated with amorphous carbon. Undisturbed slag particles of cells 1, 2, 3, 5 and 8 were analyzed with SEM using a Jeol JSM-7600F microscope (2.0 kV, LEI or SEI detector).

2.3 Batch kinetic tests

The batch kinetic test method is described in another reference (Claveau-Mallet et al., 2014) and is intended to produce exhaustion equations. The batch test included 5 identical phases. In a phase, the slag sample was placed in a 1L Erlenmeyer flask containing 350 or 700 mL of a wastewater solution. The Erlenmeyer flask was placed in a gyratory shaker at 160 rpm. The flask was closed with a rubber cap that

contained three airtight holes; one for a pH probe, one for a sampling tubing and one for a tubing connected to a N₂ gas balloon. The synthetic solution was composed of KH₂PO₄, K₂HPO₄, NaHCO₃ and CaCl₂ dissolved in tap or distilled water. Four solutions with different concentrations were used to test the method in a realistic range of wastewater types (pH of 6.5 to 7.9, o-PO₄ of 8 to 24 m P/L, Ca of 17 to 50 mg/L, TIC of 0.5 to 24 mg C/L and alkalinity of 3 to 107 mg CaCO₃/L). At time zero, slag was inserted. pH was monitored for 3 to 4 days. Three intermediary 20-mL samples were taken and analyzed for o-PO₄, filtered Ca and filtered TIC. When necessary, a linear correction against time was applied to pH measurements to account for probe drift. After this test, the slag sample was rinsed and immediately transferred to a 160 rpm shaken HNO₃ acid bath of known volume and concentration for 3 to 5 days. After the acid bath, pH was measured and the corresponding leached CaO from the slag was computed using numerical simulations (explained in section 2.5.2). After the acid bath, the slag sample was carefully rinsed and used again for a subsequent phase.

Each 300-g slag sample from cells 1 to 8 was used for a 5-phase kinetic test, resulting in 16 kinetic tests (2 replicates per cell). One-phase batch tests on dismantled column slag samples were performed for cells 1 to 9.

2.4 Model description

2.4.1 Precipitation

The model's Gujer matrix is presented in Appendix (Tables A1 and A2). Three mineral phases are included: hydroxyapatite (HAP, Ca₅(PO₄)₃OH), monetite (MON, CaHPO₄) and CAL (CaCO₃). HAP was chosen as typical end-product phosphate precipitate found in steel slag filters (Baker et al., 1998) while CAL was chosen as easily formed precipitate under calcium-rich alkaline conditions (Jung et al., 2010; Liira et al., 2009; Mayes et al., 2006). MON was chosen as an intermediary and unstable calcium phosphate phase (Valsami-Jones, 2001) based on previous results (Claveau-Mallet et al., 2014). No other

intermediary phases were included to keep the model simple. The transformation of MON into HAP (MONtoHAP) was modelled as precipitation of HAP2, an artificial phase composed of ions missing from MON before being HAP. Precipitation rates for HAP, MON and CAL were formulated with a basic expression rate = $k \times SI$, with k being a constant normalized with slag surface and SI the saturation index. The bulk solubility constant for HAP (K_{spHAP_bulk}) was set at 10^{-57} (Stumm and Morgan, 1996), within the 10^{-55} to 10^{-63} range reported in the literature (Lundager Madsen, 2008; Oelkers et al., 2009; Parkhurst and Appelo, 1999; Stumm and Morgan, 1996). K_{spCAL} was set at $10^{-7.5}$ following the calibration of the column test. This value falls between crystalline calcite ($10^{-8.48}$, PHREEQC database (Parkhurst and Appelo, 1999)) and hydrated calcium carbonate ($10^{-7.144}$, MINTEQA database (Allison et al., 1991)). K_{spMON} was set at 10^{-7} from Valsami-Jones (Valsami-Jones, 2001).

Two types of HAP were included to account for two types of precipitation. HAP_HO was HAP formed by homogeneous precipitation (new seeds precipitated in voids, or spontaneous precipitation) while HAP_HE was HAP formed by heterogeneous precipitation (on existing surfaces - crystal growth). HAP_HE occurred below a critical saturation index (SI_c) while HAP_HO occurred over SI_c . In homogeneous precipitation, crystal size was assumed to be constant. K_{spHAP_HO} was set at 10^{-46} according to an equilibrium state generally observed in various slag filter effluents when the effluent pH is above 10 with a high HRT_v (Table 1 and Figure 1). In Table 1, Ca^{2+} , OH^- and PO_4^{3-} activities were determined with PHREEQC and used for apparent solubility calculation. Studies conducted with hydrated oil shale ash were included in Table 1 as they behave in a similar way to slag. Using equation 1 for the solubility of fine particles (Stumm and Morgan, 1996), the crystal size a_{HAP_0} was calculated at 31.3 nm, assuming a temperature of 298 K. The specific surface (S_{HAP}) was calculated assuming a columnar shape for HAP and an L/D ratio (L_{HAP}) of 50. The value calculated for a_{HAP_0} is close to crystal size measured in this study (presented in a following section) and measurements made during previous studies (Claveau-Mallet et al., 2012, 2013).

$$\log(K_{spHAP_{HO}}) = \log(K_{spHAP_{bulk}}) + \frac{2}{3} \frac{V_{SHAP}}{2.3RT} \quad [1]$$

Table 1. Apparent HAP solubility from reported alkaline filter effluent with pH \geq 10, based on reported pH, Ca and o-PO₄ concentration. Resulting mean and median were 10^{-45,7} and 10^{-46,0} from 389 data points.

Material	Size (mm)	Influent	Type of study	Apparent log K _{sp} of HAP		Ref	Nb of data points
				mean	median		
Sas	5-10	Solution	lab – column	-45.55	-45.94	1	35
EAF slag	5-10	Solution	lab – column	-45.18	-45.72	2	103
Sas	2.5-5	Solution	lab – column	-48.06	-48.17	3	6
Sas	5-10	real fishfarm WW	pilot – column	-45.23	-45.39	4	46
Hydr. Oil shale ash	5-20	real domestic WW	pilot – CW	-46.32	-46.52	5	62
Hydr. Oil shale ash	5-20	real landfill leachate	pilot – CW	-46.55	-46.42	5	97
ladle furnace slag	0-1	reconst. fishfarm WW	lab – CW	-44.86	-45.28	6	9
Sas mixed with limestone	5-15	reconst. fishfarm WW	lab – CW	-46.04	-46.01	6	12
Sas mixed with limestone	20-40	reconst. fishfarm WW	lab – CW	-44.48	-44.56	6	8
Sas	10-30	reconst. domestic WW	lab – CW	-40.85	-41.01	7	11
Sas	30-100	reconst. domestic WW	lab – CW	-45.16	-45.26	7	8*
BOF oxide mixture	0.003-0.1	Solution	lab – column	-49.51	-49.47	8	8*
EAF slag	20-40	real domestic WW	pilot – CW	-44.07	-	9	* +
BOF slag	20-40	real domestic WW	pilot – CW	-43.52	-	9	* +

259 *: all data below pH 10 for these studies. Data was not considered for calculation of global K_{sp}

260 +: single K_{sp} calculated from reported mean values for pH, o-PO₄ and Ca

261 Sas: same as present study; WW: wastewater; CW: constructed wetland

262 Ref #1: Claveau-Mallet et al., 2012. Ref #2: Claveau-Mallet et al., 2013. Ref #3: Forget, 2001. Ref #4 :

263 Kõiv et al., 2016. Ref #5 : Kõiv et al., 2010. Ref #6 : Abderraja Anjab, 2009. Ref #7 : Staingart, 2012. Ref

264 #8: Baker et al., 1998. Ref #9: Barca et al., 2013.

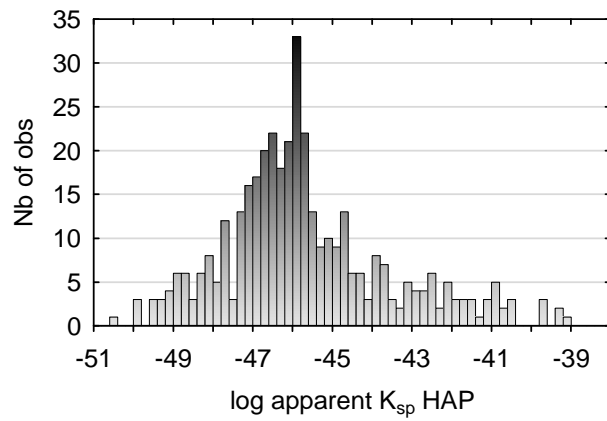


Figure 1. Apparent HAP solubility distribution for all reported studies ($\text{pH} \geq 10$; 389 observations).

In heterogeneous precipitation, crystal size is a variable following crystal growth on existing seeds, assuming that all crystals have the same size. The number of seeds (se_{HAP}) increases as homogeneous precipitation takes place, assuming an initial number of seeds (se_{HAP_0}) and columnar shape. Equations for HAP_HE specific surface and solubility product are provided in equations 2 and 3.

$$\log(K_{spHAP_HE}) = \log(K_{spHAP_bulk}) + \frac{\frac{2}{3}\gamma S_{HAP}}{2.3RT} \quad [2]$$

$$S_{HAP} = \frac{(4L_{HAP}+2)MW_{HAP}}{a_{HAP}\rho_{HAP}} \quad [3]$$

2.4.2 Slag dissolution

Slag composition was simplified to the chemical formula $\text{CaO} \cdot 0.3\text{CaCl}_2$. Exhaustion equations were determined experimentally (described later), resulting in decreasing functions for saturation pH (pH_{sat}) and dissolution kinetic constant (k_{diss}). k_{diss} was normalized with slag surface as for precipitation constants. The proposed approach gives flexibility to the model and every specific slag has its own exhaustion parameters determined from batch tests by regression.

In this model, slag dissolution is assumed to be limited by Fick's law of diffusion (Domenico and Schwartz, 1998) through a crystal barrier that forms uniformly on the slag surface in a thin layer. The

thickness of the crystal barrier (d_{barr}) increased according to CAL, HAP and MON precipitation, assuming a constant specific surface (S) for slag (equation 4). It was assumed that the type of precipitation has an influence on the diffusion coefficient (D_{barr}) and that diffusion is easier in a large and organized crystals framework, compared to numerous small crystals. Mathematically, D_{barr} was defined with a step function set initially at a high value, and to a lower value when the seed concentration was doubled. The values for low and high D_{barr} were determined by calibration (presented in the results section). As either dissolution or diffusion rate is the limiting process (the smallest), the step function was added to consider the passage from dissolution-limiting to diffusion-limiting.

$$d_{barr} = \frac{(100[CAL]+502[HAP]+136[MON]+366[HAP2]) \times n}{\rho_{barr} S(n-1)} \quad [4]$$

2.4.3 Hydraulic model

In continuous flow column simulations, the Advection-Reaction-Dispersion (ARD) equation for 1D flow was used (equation 5). A first-order exchange approximation was added to account for diffusion between effective and immobile porosity (equation 6). The hydraulic model is available in the PHREEQC software (Parkhurst and Appelo, 1999).

$$\frac{\partial C}{\partial t} = -v \frac{\partial C}{\partial x} + D^* v \frac{\partial^2 C}{\partial x^2} - \frac{\partial q}{\partial t} \quad [5]$$

$$\frac{db_{im}}{dt} = n_{im} \left(1 + \frac{dq}{dC} \right) \frac{dC_{im}}{dt} = D_n (C_e - C_{im}) \quad [6]$$

2.5 Numerical simulations

Numerical simulations were performed using the PHREEQC software with its IPHREEQC modules for interfacing with MATLAB (Charlton and Parkhurst, 2011).

2.5.1 Batch tests

The initial solution was simulated with KH_2PO_4 , K_2HPO_4 , CaCl_2 and NaHCO_3 added to pure water. A small amount of HCl or NaOH was included to reproduce the precise pH of the experimental solution. Before any simulated batch test, the solution was allowed to numerically precipitate HAP and CAL (but not MON) until equilibrium in the EQUILIBRIUM_PHASES block, to ensure that stable solutions were used for batch tests. Simulated and experimental alkalinity were used for calibration of initial solutions. Slag exhaustion was considered to be constant, therefore, pH_{sat} and k_{diss} were constant instead of being adjusted according to exhaustion equations. pH_{sat} was set as the maximum pH value reached in the experimental batch test. Calcite precipitation was removed from the batch test model, as surprisingly no calcite precipitation occurred in experimental batch tests (no TIC reduction).

The model constants were identified by minimizing the misfit between the simulated output and the experimental pH and $o\text{PO}_4$ measurements. The objective function optimization was performed on the log transformed constants k_{diss} , k_{HAP} , k_{MON} , $k_{MONtoHAP}$ and CaO_{in} with the conjugate gradient method and the golden-section search method (Press, 2007). As shown in Table 2, a two-step strategy was used to achieve satisfactory results and speed-up the calibration process. In the first step, the mean absolute error between the experimental and simulated pH (F_1) was minimized with large tolerances for PHREEQC ($1\text{E-}11$) and the optimization algorithm ($1\text{E-}7$ for line search and 0.01 as F stop criteria). Then, the objective function F_2 was minimized with more demanding tolerances ($1\text{E-}12$ for PHREEQC and line search, and 0.001 as F stop criteria). Note that CaO_{in} was a little amount of CaO instantaneously released at the water/slag contact, added for improving the calibration.

Table 2. Batch test inversion parameters for conjugate gradient method

Step	Initial values (log)	Objective function
1	-7 for k_{diss} and CaO_{in} -6.5 for k_{MON} -9 for k_{HAP} and $k_{MONtoHAP}$	$F_1 = \frac{1}{n} \sum_{i=1}^n pH_{i,exp} - pH_{i,sim} $

2	Solution from inversion 1	$F_2 = F_1 + \frac{0.2}{m} \sum_1^m oPO_{4m,exp} - oPO_{4m,sim} $
---	---------------------------	--

321

322 2.5.2 Exhaustion functions

323 Exhaustion functions were produced by plotting pH_{sat} and k_{diss} against total leached CaO ($CaOl_{TOT}$).

324 For a given phase i , $CaOl_{TOT}^i$ was calculated by cumulating leached CaO in preceding kinetic tests and

325 acid bath (equation 7). $CaOl_{BATH}$ was determined by simulating acid bath with PHREEQC, following the

326 final pH of the acid bath as a target value.

$$327 \quad CaOl_{TOT}^i = 0.5 \times CaOl_{KTEST}^i + \sum_{n=1}^{i-1} (CaOl_{KTEST}^n + CaOl_{BATH}^n) \quad [7]$$

328 Exhaustion functions coefficients were determined by linear regression of pH_{sat} vs $CaOl_{TOT}$ (equation

329 8) and logistic function regression of k_{diss} vs $CaOl_{TOT}$ (equation 9). Mean regression coefficients were

330 kept for k_{diss} , but coefficients following the top of the graphical data cloud were kept for pH_{sat} , as

331 pH_{sat} is a saturation state, and we can assume that saturation is controlled by the most reactive

332 particles.

$$333 \quad pH_{sat} = P_2 - \frac{P_2 - P_1}{(1 + e^{-P_3(CaOl_{TOT} - P_4)})} \quad [8]$$

$$334 \quad k_{diss} = B_1 + B_2 CaOl_{TOT} \quad [9]$$

335 In the Gujer matrix, exhaustion functions included additional terms involving porosity and slag density to

336 account for the conversion of $CaOl_{TOT}$ (units of mol/g slag) into X_{CaO} (units of mol/L water) for filter

337 numerical simulations.

338 2.5.3 Column test

339 The simulated influent was prepared according to the procedure described in the batch tests section.

340 The column test was simulated within KINETIC and TRANSPORT blocks, with 50 numerical cells and a

tolerance of 1E-6. Kinetic rates were applied to both mobile and immobile cells. Hydraulic parameters

n_e , D^* and D_n were calibrated with each tracer test.

3 Results and discussion

3.1 Determination of exhaustion equations and precipitation constants

In general, batch test calibration was good, except for the period 0 to 100 min where the model

overestimated slightly the o-PO₄ concentration. The calibration quality was considered satisfactory for

pH if the simulated pH followed the experimental pH-rise (sometimes with an overlap of curves).

Simulated o-PO₄ was considered satisfactory if it reproduced approximatively the concentration drop at

the beginning of the test and reproduced accurately the data point at the end of test (close to

equilibrium). The mean error function was $F_2 = 0.24$ for all batch tests. An example of a well-calibrated

batch test (rank 7 out of 84 for global error function) is shown in Figure 2. No TIC reduction was

observed. Absence of CAL precipitation in batch tests was not expected, as calcite was precipitated in

column tests and is frequently observed in slag filters (Claveau-Mallet et al., 2013; Liira et al., 2009).

Mean precipitation constants were $k_{HAP} = 10^{-11.03} \text{ mol HAP/s m}^2 \text{ slag}$,

$k_{MON} = 10^{-8.67} \text{ mol MON/s m}^2 \text{ slag}$ and $k_{MONtoHAP} = 10^{-8.01} \text{ mol HAP2/s mol MON}$.

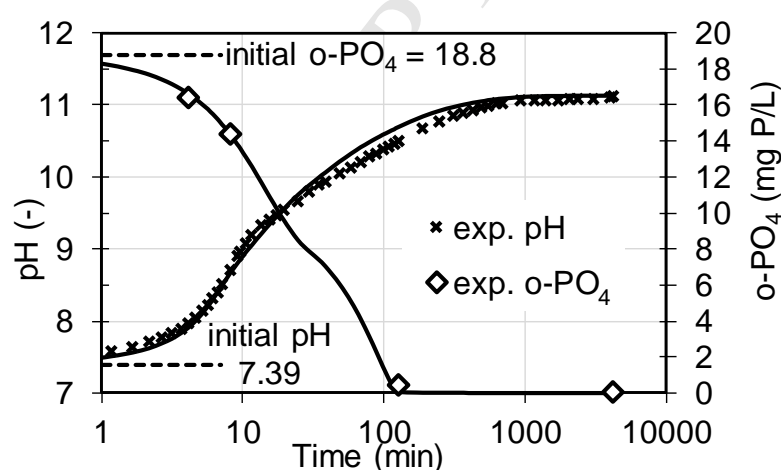


Figure 2. Example of a batch test calibration. Simulated data is shown with lines. Batch test error

functions: 0.09 for pH and 0.15 for o-PO₄.

pH_{sat} and k_{diss} obtained from all batch tests were plotted against CaOl_{tot} for the production of exhaustion

functions (Figure 3). For k_{diss} , linear regression coefficients were used in column simulations ($B_1 = -7.91$

and $B_2 = -1933$ g/mol, see equation A8). pH_{sat} exhaustion function had to be slightly increased above the

data cloud (discussed later) to improve the calibration (Figure 3B), resulting in coefficients $P_1 = 9.1$, $P_2 =$

12.1, $P_3 = 6000$ and $P_4 = 1.2E-4$ (see equation A7).

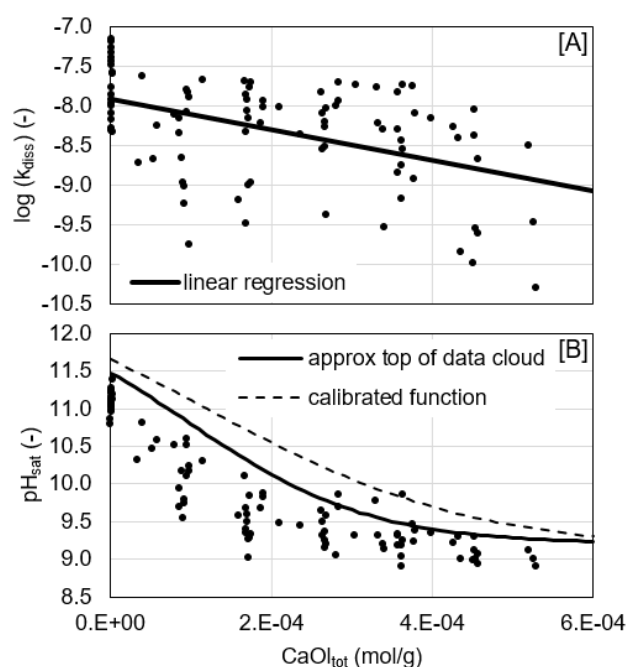


Figure 3. Exhaustion functions for k_{diss} (A) and pH_{sat} (B). Regression coefficients are provided in text.

3.2 Column test calibration

An example of tracer test calibration is shown in appendix. Hydraulic parameters D^* (dispersivity) and

D_n (exchange factor between mobile and immobile porosity) were roughly constant for 8 tracer tests,

while effective porosity (n_e) decreased slightly following the column operation. The n_e decrease was

neglected, and hydraulic parameters from tracer test at time 187 were used ($n_e = 0.359$, $D^* = 5$ cm and $D_n = 5 \times 10^{-6} \text{ s}^{-1}$).

Results of numerical simulations are compared to experimental data in Figure 4. pH was correctly predicted for cells 1 to 6 but slightly underestimated for cells 7 to effluent. o-PO₄ was in general successfully predicted, except for cells 1 and 2 in the first 100-200 days, where the o-PO₄ rise was predicted too late. This could be explained by the close position of cells 1 and 2 relative to the influent point resulting in a non plug flow condition for these cells and in some short-circuiting. Calibration of o-PO₄ from cells 5 to 7 was less accurate for the last 100 days, as the model predicted a stable concentration while the experiment showed an increase of almost an order of magnitude. Calcium and TIC calibration were less accurate than those for pH and o-PO₄, but were considered satisfactory. The o-PO₄ removal efficiency increase induced by the inflow rate reduction at 517 days was correctly predicted by the model.

Calibrated constants were $k_{CAL} = 10^{-9} \frac{\text{mol CAL}}{\text{s m}^2}$, $SI_c = 0.2$ and $\rho_{barr} = 2000 \frac{\text{kg}}{\text{m}^3}$. Precipitation constants for HAP, MON and MONtoHAP were already determined in batch tests and were not changed for column simulations. SI_c was lower than reported values for calcite, which occurs in heterogeneous precipitation over $SI_c = 0.3$ and homogeneous precipitation over $SI_c = 1.5$ (Mayes et al., 2006). ρ_{barr} value was similar to dry density for a natural sand. k_{CAL} was 2.5 orders of magnitude higher than the initial value of 10^{-5} M/s reported by Mbamba, Tait et al. (2015), and monetite constant was in the same order of magnitude as Mbamba's values. In Mbamba's study, precipitation rates were function of crystal concentration, with initial crystal seeds of $1\text{E-}5 \text{ M}$, while the effect of crystal concentration was not considered in the P-Hydroslog model precipitation rates.

The column was divided in two zones for the calibration of se_{HAP_0} : cells 1 to 6 were set at $2\text{e}21$ seeds/L and cells 7 to 9 (and all immobile cells) were set at $5\text{e}20$ seeds/L. This refinement was necessary to achieve both o-PO₄ calibration of first cells (mainly homogeneous precipitation) and last cells (mainly

heterogeneous precipitation). Attributing different se_{HAP_0} values for two zones was considered realistic because it represents a crystal behavior in which at a very low supersaturation index, fewer but bigger crystals are formed. This behavior was confirmed during column dismantling. In cells 8 and 9, a very small amount of precipitates was observed and sampled, with fresh- and unused-looking slag. Several well-formed crystals could be seen by naked eyes only in cells 8 and 9 (3-4 mm in length).

The implementation of the diffusion equation is considered a major improvement compared to previous prototype versions of the model. Without the diffusion equation, CaO would always be leached at its maximum capacity (pH_{sat}) and longevity would be highly overestimated (see the validation section).

D_{barr} calibration was $1E-10$ m²/s at first and was decreased to $5E-16$ m²/s when the seed concentration was doubled. Calibrated values of D_{barr} for the two steps are similar to diffusion coefficients observed for clays. A large range was reported for radioactive waste storage applications: from 10^{-17} to $> 10^{-13}$ m²/s in consolidated clay (Alonso et al., 2009) and 10^{-11} to 10^{-10} m²/s in altered bentonite (Manjanna et al., 2009).

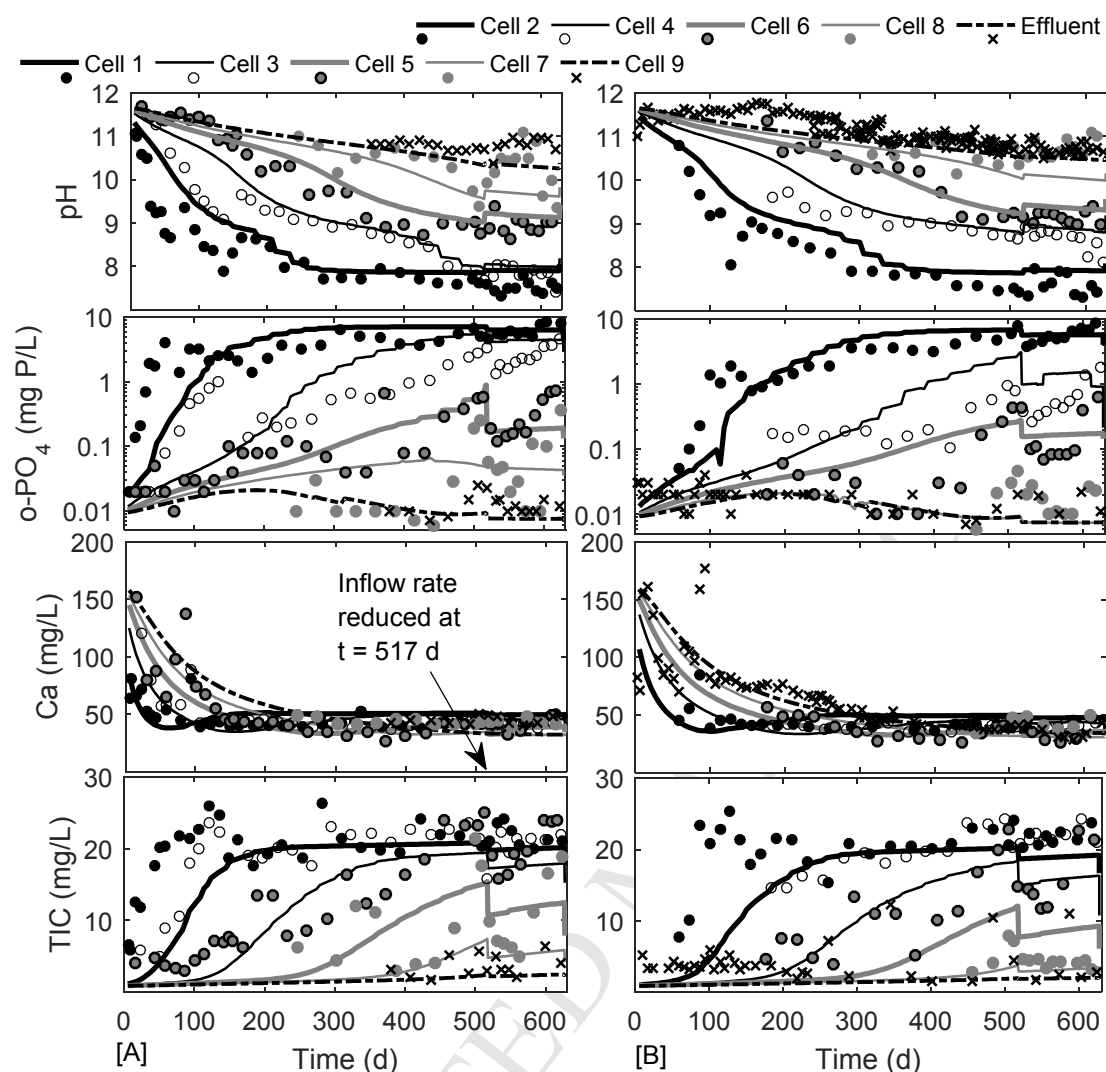


Figure 4. Water composition in a column test for cells 1 to 9 (A) and cells 2 to effluent (B). Experimental data is shown with dots or x and simulated data with lines.

3.3 Study of model precipitation hypothesis

The appropriateness of the diffusion equation can be assessed by the robustness of the model regarding pH. The model could predict pH at the end of operation, pH after the 6-day rest and pH_{sat} (Figure 5). pH was slightly underestimated for pH_{sat} and pH after rest, but relative trends for pH and pH_{sat} were properly predicted, as well as the pH increase induced by the 6-day rest. The crystal layer was realistic as

uniform crystal deposits were observed by SEM (Figure 6). The presence of cracks induced by air-drying was also suggesting that a crystal suspension layer was present onto the slag surface. Uniformity of crystal composition was confirmed by TEM-EDS as CAL and HAP were frequently found in the same crystal at nanometric scale.

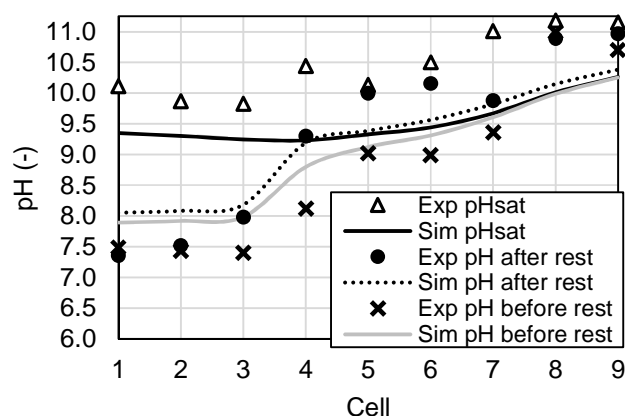


Figure 5. pH distribution within column at the end of operation (623 days of feeding followed by 6 days of rest).

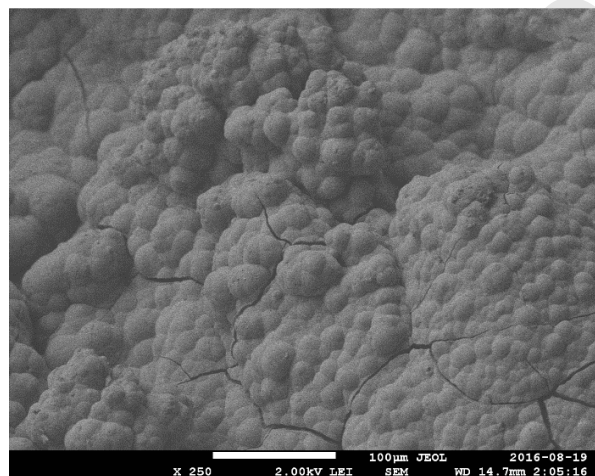


Figure 6. SEM picture of slag grain surface from cell 2 at dismantling.

Crystal size in homogeneous precipitation was confirmed by microscope observations. In cells 1 to 3, where the amount of precipitated HAP was sufficient for measurements, isolated crystals in TEM

pictures were measured, resulting in a 35 nm mean value for 505 measurements. A similar value of 24 nm was calculated from XRD diffractograms of cells 1 to 3. No specific increase was observed in crystal size from cells 1 to 3, validating the constant crystal size hypothesis for homogeneous precipitation. HAP composition was confirmed by XRD patterns (provided in supporting information). HAP composition for individual crystals from TEM was confirmed by P and Ca presence with EDS. No monetite was detected by XRD and no monetite precipitation occurred in the column simulations while monetite was precipitated in batch test simulations, suggesting that pH rise in column was too fast for monetite formation. The distribution of mineral phases within the simulated column is shown Figure 7. Hydroxyapatite was mainly formed by homogeneous precipitation in the first cells, while heterogeneous precipitation represented a small amount of precipitates. Cells were progressively filled over time and precipitates were concentrated in the first 3 cells after 300 d and in the first 5 cells after 626 days. The calcite concentration within the column was higher than the hydroxyapatite concentration.

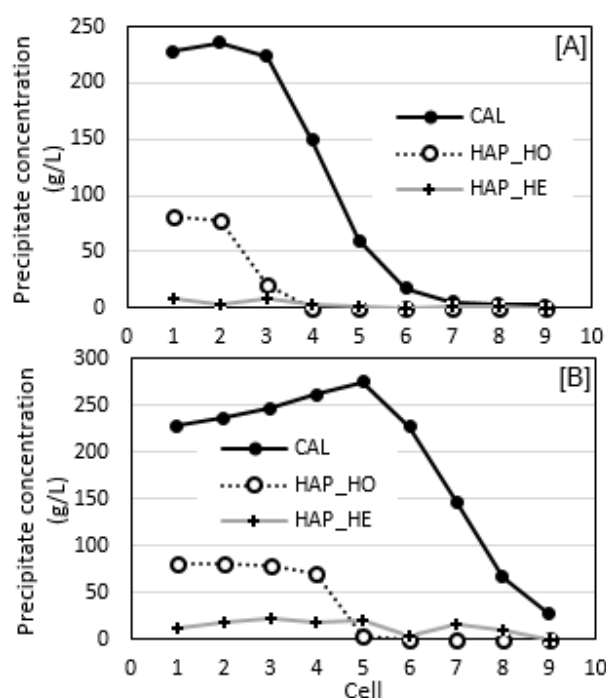


Figure 7. Distribution of precipitates in the simulation after 300 d (A) and 626 d (B).

The relative small amount of formed HAP in heterogeneous precipitation made impossible XRD or TEM crystal size analysis for heterogeneous HAP. It was possible, however, to analyse the progression of calcite crystal size within the column using XRD. Its size was around 200 nm in cells 1 to 3, increased to 900 nm in cell 5, and was over the limit of Scherrer equation in cells 6 and higher. This suggests homogeneous precipitation and constant size in the first cells and heterogeneous precipitation and crystal growth in last cells.

Even if homogeneous and heterogeneous precipitation was experimentally observed for calcite, only homogeneous precipitation was included in the model. Assuming homogeneous precipitation at 200 nm (as measured in cells 1 to 3) and spherical crystals, the computed solubility product from equation 1 is very close to bulk solubility. While HAP growth decreases its solubility, CAL homogeneous crystals are large enough to neglect this effect.

3.4 Preliminary validation of the P-Hydroslog model

A preliminary validation of the model was performed using experimental data from a pilot test consisting of steel slag columns fed with a real fish farm effluent (Figure 8; Kõiv et al., 2016). In this pilot test, the steel slag column was operated at an HRT_v of 15 h and fed in two sequential phases, first with a low-strength influent and second with a high-strength one (phase 1: chemical oxygen demand of 10 mg/L, total suspended solids of 3 mg/L, total phosphorus of 2.6 mg P/L and alkalinity of 50 mg $CaCO_3$ /L; phase 2: chemical oxygen demand of 1713 mg/L, total suspended solids of 340 mg/L, total phosphorus of 31 mg P/L and alkalinity of 1000 mg $CaCO_3$ /L). The P-Hydroslog model resulted in a pH curve similar to that of the prototype model, but the $o-PO_4$ prediction was improved. The P-Hydroslog model predicted a longevity (e.g. reaching 1 mg P/L) of less than 50 d in the high-strength influent (Figure 8, dashed line). In the previous version, a longevity of 1 year at an HRT_v of 30 h had been predicted (Kõiv et al., 2016) for the high-strength influent, which is too high considering the fast breakthrough in experimental data (Figure 8). In the present validation work, the implementation of heterogeneous precipitation was not

necessary, and even led to decreasing o-PO₄ curve that did not follow the experimental data (Figure 8, grey line). It shows the need for further work regarding heterogeneous and homogeneous precipitation in steel slag filters.

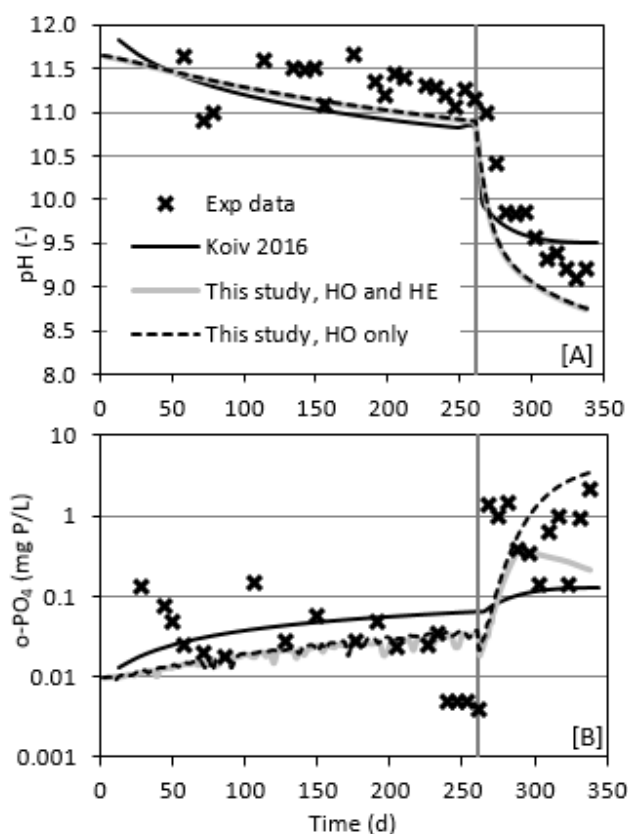


Figure 8. Validation of the P-Hydroslag model with data from Kõiv et al. (2016), column CS2A.

Simulations are compared to simulations with a prototype version from Kõiv et al. (2016). Simulated results are presented with lines. The vertical line indicates the change of influent from a low strength (0-260 d) to a high -strength influent (260-350 d).

3.5 Model limitations and recommendations

The main issue regarding the model is the number of batch kinetic tests needed to provide exhaustion equations. The hypothesis of most reactive grains in batch tests conditioning column tests should also be examined, because even if pH_{sat} exhaustion equation was overestimating experimental data, pH in

the last cells of columns were underestimated. Work should be done using statistical analysis and theory of artificial granular material sampling (Gy, 1979) for reducing the number of batch tests and transposing correctly batch to column conditions. The method for measurement of exhaustion functions should also be tested with other types of alkaline slag to test its relevance. The method is expected to be suitable for other types of alkaline slag as basic oxygen furnace slag, blast furnace slag or other alkaline granular materials such as oil shale fly ash.

Calibration of heterogeneous precipitation was limited by experimental data, as last cells did not reach their longevity. Additional studies involving long-term operation of slag filters and breakthrough of last sections of filters, in which heterogeneous precipitation occurred for a while, would be needed for accurate calibration and in-depth study of seeds concentration and type of precipitation. In this paper, two layers of different seeds concentration were proposed, but other formulations would be possible including step functions for seeds VS saturation index, increasing the number of layers or adding a third type of HAP.

Further work should be conducted regarding need for refinement of the model. Additional features such as interaction with atmospheric CO₂ or porosity reduction (Courcelles et al., 2011) may be needed in some cases as constructed wetlands. The model could be improved with additional P species (Mbamba, Tait, et al., 2015) or consideration of crystal surface in rate equations. Crystal surface is obviously increasing in this type of process, with long operation time without extraction, but kinetic parameters may be less important than saturation parameters (pH_{sat} and K_{spHAP_HE}). Sensitivity analyses would be needed to assess which aspect should be studied further, slag dissolution kinetics, crystal equilibrium parameters or crystal kinetic parameters. The model must also be tested under real wastewater conditions. A model validation with data from pilot steel slag filters fed with real wastewater is currently in progress by the authors research team.

3.6 Use of the P-Hydroslog model in practical applications

The use of the P-Hydroslog model in practical applications requires some data collection and calibration work. The calibration of the influent should focus on accurate reproduction of alkalinity and of inorganic carbon concentration, as they contribute significantly to the filter exhaustion. In applications in which the influent is a secondary effluent, the alkalinity concentration is influenced mainly by the type of tap water source (e.g. groundwater or surface water) and upstream process control (e.g. addition of bicarbonate). Important seasonal fluctuations in alkalinity may also be caused by fluctuations in upstream wastewater treatment nitrification.

The exhaustion functions of the reactive material should be measured. Further work is needed to assess if existing exhaustion functions can be reused in other applications with the same media, as suggested by analyzing results from previous work (Section 3.4, Kõiv et al., 2016). Further work is also needed to assess if exhaustion functions can be transposed on the basis of specific surface area using a given media that has different sizes of grains.

The main calibration effort in future uses of the P-Hydroslog model should be to assess if heterogeneous precipitation is needed when working with real wastewater applications. In any cases, the diffusion coefficient D_{barr} may need to be recalibrated. Calibration efforts should focus on parameters that affect pH as pH_{sat} and D_{barr} .

4 Conclusion

The first version of the P-Hydroslog model that can be used for prediction of steel slag filter efficiency and longevity was presented in this paper. The objectives were to calibrate the model with experimental data and evaluate the validity and realism of the model. The main outcomes were as follows:

- A complete model equation matrix was provided. The model included two main kinetic equation sets: a first set for CaO dissolution and a second set for precipitation. CaO dissolution equations included slag exhaustion and CaO diffusion through a uniform crystal barrier on slag particles.

Precipitation equations included calcite precipitation, monetite precipitation, transformation of monetite into hydroxyapatite, homogeneous hydroxyapatite precipitation (constant size) and heterogeneous hydroxyapatite precipitation (increasing size). An equation for hydroxyapatite solubility related to crystal size was included. Standard equilibrium reactions were included in the model via the PHREEQC software. The advection-diffusion-reaction model was used as the hydraulic model (1D porous media transport).

- The crystal barrier hypothesis was confirmed by SEM observations of used slag grains. Homogeneous and heterogeneous precipitation hypothesis was confirmed by TEM crystal size count and XRD measurements.
- The model was validated with an independent data set from a pilot test in which real wastewater conditions we used.
- The model was successful in producing realistic results. A simple and flexible experimental method was presented for the measurement of exhaustion functions, which are parameters suitable for a mechanistic model. This empirical method is interesting because it overcomes the complex task of relating slag composition to filter behavior. Numerical simulations reproduced experimental breakthrough curves (pH, o-PO₄, Ca, TIC) of an upward flow column slag filter.

ACKNOWLEDGMENT

The authors warmly thank Denis Bouchard, Manon Leduc, Simon Allaire, Simon Amiot and Patricia Bove from Polytechnique Montreal for chemical analyses and technical assistance. They also thank Margit Kõiv-Vainik, from University of Tartu, for providing constructive comments on the manuscript. A special thank is given to Jean-Philippe Massé and Philippe Plamondon, from Polytechnique Montreal CM² lab, for their assistance with TEM, XRD and SEM analysis. Slag material was provided by Philippe Bouchard, from Minéraux Harsco. This project was funded by the Natural Sciences and Engineering Research Council of Canada.

547 REFERENCES

- 548 Abderraja Anjab, Z. 2009. Development of a steel slag bed for phosphorus removal from
549 fishfarm wastewater (In French). M. Sc. A. thesis, Polytechnique Montreal, Montreal,
550 Canada.
- 551 Allison, J. D., Brown, D. S., Novo-Gradac, K. J. 1991. *MINTEQA2/PRODEFA2, a geochemical*
552 *assessment model for environmental systems: version 3.0 user's manual*. Environmental
553 research laboratory, USEPA, Athens, Georgia.
- 554 Alonso, U., Missana, T., Garica-Gutiérrez, M., Patelli, A., Siitari-Kauppi, M., Rigato, V. 2009.
555 Diffusion coefficient measurements in consolidated clay by RBS micro-scale profiling.
556 Applied Clay Science 43, 477-484.
- 557 American Public Health Association, American Water Works Association, Water Environment
558 Federation. 2012. Standard methods for the examination of water and wastewater 22nd
559 ed. Washington, D. C.
- 560 ASTM. 2004. ASTM C127-04 Standard Test Method for Density, Relative Density (Specific
561 Gravity), and Absorption of Coarse Aggregate. ASTM International: West Conshohocken,
562 PA.
- 563 ASTM. 2011. ASTM C 702 / C 702 M-11 Standard Practice for Reducing Samples of Aggregate to
564 Testing Size. ASTM International: West Conshohocken, PA.
- 565 Baker, M. J., Blowes, D. W., Ptacek, C. J. 1998. Laboratory development of permeable reactive
566 mixtures for the removal of phosphorus from onsite wastewater disposal systems.
567 Environmental Science and Technology 32(15), 2308-2316.
- 568 Barca, C., Troesch, S., Meyer, D., Drissen, P., Andrès, Y., Chazarenc, F. 2013. Steel slag filters to
569 upgrade phosphorus removal in constructed wetlands: two years of field experiments.
570 Environmental Science and Technology 47(1), 549-556. doi:10.1021/es303778t
- 571 Charlton, S. R., Parkhurst, D. L. 2011. Modules based on the geochemical model PHREEQC for
572 use in scripting and programming languages. Computers & Geosciences 37(10), 1653-
573 1663.
- 574 Chazarenc, F., Kacem, M., Gérente, C., Andrès, Y. 2008. 'Active' filters: a mini-review on the
575 use of industrial by-products for upgrading phosphorus removal from treatment
576 wetlands. In: Proceedings of the 11th Int. Conf. on Wetland Systems for Water Pollution
577 Control. International Water Association, Indore, India, November 1-7.
- 578 Claveau-Mallet, D., Courcelles, B., Comeau, Y. 2014. Phosphorus removal by steel slag filters:
579 Modeling dissolution and precipitation kinetics to predict longevity. Environmental
580 Science and Technology 48(13), 7486-7493.
- 581 Claveau-Mallet, D., Lida, F., Comeau, Y. 2015. Improving phosphorus removal of conventional
582 septic tanks by a recirculating steel slag filter. Water Quality Research Journal of Canada
583 50(3), 211-218.
- 584 Claveau-Mallet, D., Wallace, S., Comeau, Y. 2012. Model of phosphorus precipitation and crystal
585 formation in electric arc furnace steel slag filters. Environmental Science and Technology
586 46(3), 1465-1470. doi:10.1021/es2024884
- 587 Claveau-Mallet, D., Wallace, S., Comeau, Y. 2013. Removal of phosphorus, fluoride and metals
588 from a gypsum mining leachate using steel slag filters. Water Research 47(4), 1512-
589 1520.

- Courcelles, B., Modaressi-Farahmand-Razavi, A., Gouvenot, D., Esnault-Filet, A. 2011. Influence of precipitates on hydraulic performance of permeable reactive barrier filters. *International Journal of Geomechanics* 11(2), 142-151.
- Cullity, B. D. 2001. Diffraction III: Real Samples. In: *Elements of x-ray diffraction* 3rd ed. Upper Saddle River, NJ: Prentice Hall.
- Domenico, P. A., Schwartz, F. W. 1998. *Physical and Chemical Hydrogeology* 2nd ed. New York: John Wiley & sons.
- Forget, C. 2001. Dissolved phosphorus removal from fish farm effluents by reactive granular media (in French). M. Sc. A. thesis, Polytechnique Montreal, Montreal, Canada.
- Gy, P. 1979. *Developments in geomathematics. theory and practice 4, Sampling of particulate materials*. New York: Elsevier Scientific Publications.
- Jung, W.-M., Kang, S. H., Kim, K.-S., Kim, W.-S., & Choi, C. K. 2010. Precipitation of calcium carbonate particles by gas-liquid reaction: morphology and size distribution of particles in Couette-Taylor and stirred tank reactors. *Journal of Crystal Growth*, 312, 3331-3339.
- Kadlec, R. H., Wallace, S. 2009. *Treatment Wetlands* 2nd ed. Boca Raton, FL: CRC Press.
- Klein, C., Dutrow, B. D., Dwight, K. J. 2002. *The 22nd edition of the manual of mineral science*. New York, NY: Wiley.
- Kõiv, M., Liira, M., Mander, Ü., Mötlep, R., Vohla, C., Kirsimäe, K. 2010. Phosphorus removal using Ca-rich hydrated oil shale ash as filter material - The effect of different phosphorus loadings and wastewater compositions. *Water Research* 44(18), 5232- 5239.
- Kõiv, M., Mahadeo, K., Brient, S., Claveau-Mallet, D., Comeau, Y. 2016. Treatment of fish farm sludge supernatant by aerated filter beds and steel slag filters - effect of organic loading rate. *Ecological Engineering* 94, 190-199.
- Liira, M., Kõiv, M., Mander, Ü., Mötlep, R., Vohla, C., Kirsimäe, K. 2009. Active filtration of phosphorus on Ca-rich hydrated oil shale ash: Does longer retention time improve the process? *Environmental Science and Technology* 43(10), 3809-3814. doi:10.1021/es803642m
- Lizarralde, I., Fernández-Arévalo, T., Brouckaert, C., Vanrolleghem, P., Ikumi, D. S., Ekama, G. A., Ayesa, E., Grau, P. 2015. A new methodology for incorporating physico-chemical transformations into multi-phase wastewater treatment process models. *Water Research* 74, 239-256.
- Lowell, S., Shields, J. E., Thomas, M. A., Thommes, M. 2004. *Characterization of Porous Solids and Powders: Surface Area, Pore Size and Density*. New York: Springer Ed.
- Lundager Madsen, H. E. 2008. Influence of foreign metal ions on crystal growth and morphology of brushite (CaHPO₄, 2H₂O) and its transformation to octacalcium phosphate and apatite. *Journal of Crystal Growth* 310(10), 2602-2612.
- Manjanna, J., Kozaki, T., Sato, S. 2009. Fe(III)-montmorillonite: basic properties and diffusion of tracers relevant to alteration of bentonite in deep geological disposal. *Applied Clay Science* 43, 208-217.
- Mayes, W. M., Younger, P. L., Aumônier, J. 2006. Buffering of Alkaline Steel Slag Leachate across a Natural Wetland. *Environmental Science and Technology* 40, 1237-1243.
- Mbamba, C. K., Batstone, D. J., Flores-Alsina, X., Tait, S. 2015. A generalised chemical precipitation modelling approach in wastewater treatment applied to calcite. *Water Research* 68, 342-353.

- Mbamba, C. K., Tait, S., Flores-Alsina, X., Batstone, D. J. 2015. A systematic study of multiple minerals precipitation modelling in wastewater treatment. *Water Research* 85, 359-370.
- Oelkers, E. H., Bénézech, P., Pokrovski, G. S. 2009. Thermodynamic Databases for Water-Rock Interaction. In: *Thermodynamics and kinetics of water-rock interaction* (Vol. 70, pp. 1-46). Chantilly, VA: Mineralogical Society of America and Geochemical Society.
- Parkhurst, D. L., Appelo, C. A. J. 1999. *User's guide to PHREEQC (Version 2) - A computer program for speciation, batch-reaction, one-dimensional transport, and inverse geochemical calculations*. (Water-Resources Investigations Report 99-4259). U. S. Geological Survey, Denver.
- Penn, C., Bowen, J., McGrath, J., Nairn, R., Fox, G., Brown, G., Wislon, S., Gill, C. 2016. Evaluation of a universal flow-through model for predicting and designing phosphorus removal structures. *Chemosphere* 151, 345-355.
- Press, W. H. 2007. *Numerical recipes: the art of scientific computing* 3rd ed. Cambridge: Cambridge University Press.
- Staingart, A. 2012. Phosphorus removal from septik tank effluents by coarse steel slag. M. Ing. thesis, Polytechnique Montreal, Montreal, Canada.
- Stumm, W., Morgan, J. J. 1996. *Aquatic Chemistry: Chemical Equilibria and Rates in Natural Waters* 3rd ed. New York: John Wiley & Sons.
- Valsami-Jones, E. 2001. Mineralogical controls on phosphorus recovery from wastewaters. *Mineralogical Magazine* 65(5), 611-620. doi:10.1180/002646101317018433
- Vohla, C., Kõiv, M., Bavor, H. J., Chazarenc, F., Mander, Ü. 2011. Filter materials for phosphorus removal from wastewater in treatment wetlands-A review. *Ecological Engineering* 37(1), 70-89.

Appendix

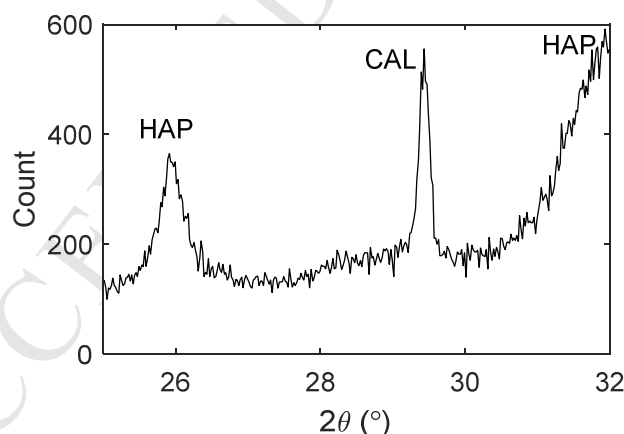


Figure A1. XRD pattern of precipitates sampled in cell #2. Main peaks of HAP and CAL diffractograms are indicated in the figure

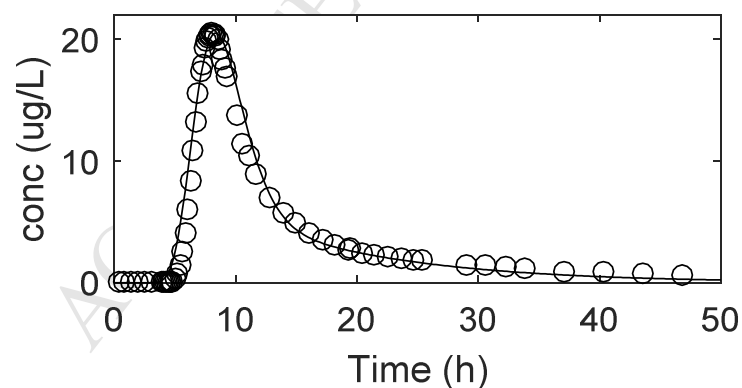
Table A1. P-Hydrosrag model matrix

Phase	Stoichiometry - aqueous						Stoichiometry – mineral phases				Rate equation	Equilibrium constants
	H^+	OH^-	Ca^{2+}	CO_3^{2-}	PO_4^{3-}	Cl^-	HAP	MON	CAL	HAP2		
Primary homogenous hydroxyapatite (HAP_HO)		-1	-5		-3		+1				$r_{HAP_HO} = 0.001k_{HAP}S \frac{(1-n)}{n} (SI_{HAP_HO})(SF_{HAP_HO})$ $SI_{HAP_HO} = \log \left(\frac{\{Ca^{2+}\}^5 \{PO_4^{3-}\}^3 \{OH^-\}}{K_{spHAP_HO}} \right)$ $SF_{HAP_HO} = \frac{1}{1 + e^{-50(\log(SI_{HAP_HO}) - \log(SI_c))}}$	$pK_{spHAP_HO} = 46$
Primary heterogeneous hydroxyapatite (HAP_HE)		-1	-5		-3		+1				$r_{HAP_HE} = 0.001k_{HAP}S \frac{(1-n)}{n} (SI_{HAP_HE})(SF_{HAP_HE})$ $SI_{HAP_HE} = \log \left(\frac{\{Ca^{2+}\}^5 \{PO_4^{3-}\}^3 \{OH^-\}}{K_{spHAP_HE}} \right)$ $SF_{HAP_HE} = 1 - \frac{1}{1 + e^{-50(\log(SI_{HAP_HO}) - \log(SI_c))}}$	$\log(K_{spHAP_HE}) = \log(K_{spHAP_bul}) + \frac{2}{3}\gamma S_{HAP}$ $+ \frac{2}{2.3RT}$
Monetite (MON)	-1		-1		-1			+1			$r_{MON} = 0.001k_{MON}S \frac{(1-n)}{n} \log \left(\frac{\{Ca^{2+}\}\{HPO_4^{2-}\}}{K_{spMON}} \right)$	$pK_{spMON} = 7$
Calcite (CAL)			-1	-1					+1		$r_{CAL} = 0.001k_{CAL}S \frac{(1-n)}{n} \log \left(\frac{\{Ca^{2+}\}\{CO_3^{2-}\}}{K_{spCAL}} \right)$	$pK_{spCAL} = 6.8$
Secondary hydroxyapatite* (HAP2)		-2	-4		-2					+1	$r_{MONtoHAP} = k_{MONtoHAP}SI_{HAP_HO}[MON]$	$pK_{spHAP_HO} = 46$

*: transformation of monetite into hydroxyapatite

Table A1 (followed). Complete P-Hydrosrag model matrix

Slag dissolution		+2	+1.3			+0.3					$r_{diss} = A(SF_{diss})$ $A = 0.001k_{diss}S \frac{(1-n)}{n} \left(\frac{pH_{sat} - pH}{pH_{sat}} \right)$ $SF_{diss} = 1 - \frac{1}{1 + e^{-50(A-B)}}$	N/A
CaO diffusion through crystal barrier		+2	+1								$r_{diff} = B(SF_{diff})$ $B = \frac{0.5D_{barr}(10^{pH_{sat}-14} - \{OH^-\})}{d_{barr}} \left(\frac{S0.001(1-n)}{n} \right)$ $SF_{diff} = \frac{1}{1 + e^{-50(A-B)}}$ $\log(D_{barr}) = -10 - 5.3 \left(\frac{1}{1 + e^{-50 \left(\frac{Se_{HAP}}{Se_{HAP_0} - 2} \right)}} \right)$	N/A

**Figure A2.** Tracer test experimental data (circles) and numerical calibration (line) (started at Time = 187 d of filter operation)

1 **Table A2.** Parameters used in the P-Hydroslag model

Parameters	Units	Value	Value obtained from
a_{HAP_0}	nm	31.3	Equation of solubility of fine particles, assuming K_{spHAP_HO} and L_{HAP}
B_1	mol CaO/m ² slag	-7.91	Experimental measurement of exhaustion functions
B_2	g/m ²	-1933	
D^*	cm	5	Calibration of tracer test
$D_{barr}HO$	m ² /s	5E-16	Calibration of column test
$D_{barr}HE$	m ² /s	10 ⁻¹⁰	Calibration of column test
D_n	s ⁻¹	5E-6	Calibration of tracer test
k_{CAL}	mol CAL/s m ² slag	10 ⁻⁹	Calibration of column test
k_{HAP}	mol HAP/s m ² slag	10 ⁻¹¹	Calibration of batch tests
k_{MON}	mol MON/s m ² slag	10 ^{-8.7}	Calibration of batch tests
$k_{MONtoHAP}$	M HAP2/(M MON s)	10 ⁻⁸	Calibration of batch tests
K_{spCAL}	M ²	10 ^{-7.5}	Calibration of column test
K_{spHAP_bulk}	M ⁹	10 ⁻⁵⁷	Literature (Stumm and Morgan, 1996)
K_{spHAP_HO}	M ⁹	10 ⁻⁴⁶	Mean value from analyse of past literature (Table 1)
K_{spMON}	M ²	10 ⁻⁷	Literature (Valsami-Jones, 2001)
L_{HAP}	-	50	Assumed (validated by TEM images)
MW_{HAP}	g/mol	502	Mineralogical tables (Klein et al., 2002)
n	-	0.492	Measured from known mass and density
n_e	-	0.359	Calibration of tracer test
n_{im}	-	0.133	Calibration of tracer test
P_1	-	9.1	Experimental measurement of exhaustion functions
P_2	-	12.1	
P_3	g/mol	6000	
P_4	mol/g	1.2E-4	
R	J mol ⁻¹ K ⁻¹	8.31	Ideal gas constant
S	m ² /g	0.308	Measured
se_{HAP_0}	seeds/L	2e21 (cells 1 to 6) and 5e20 (cells 7 to 9)	Calibration of column test
SI_c	-	0.2	Calibration of column test
T	K	298	Measured
γ	mJ/m ³	87	Literature (Stumm and Morgan, 1996)
ρ_{barr}	kg crystal/m ³	2000	Calibration of column test
ρ_{HAP}	kg/m ³	3600	Mineralogical tables (Klein et al., 2002)
ρ_{slag}	g/mL	3.8	Measured

2

3

4

Detailed equations to complement the model matrix

Advection-reaction-dispersion (ARD) equation for 1D transport and First-order exchange approximation between effective and immobile porosity:

$$\frac{\partial C}{\partial t} = -v \frac{\partial C}{\partial x} + D^* v \frac{\partial^2 C}{\partial x^2} - \frac{\partial q}{\partial t} \quad [A1]$$

$$\frac{db_{im}}{dt} = n_{im} \left(1 + \frac{dq}{dC} \right) \frac{dC_{im}}{dt} = D_n (C_e - C_{im}) \quad [A2]$$

Detailed equations for HAP_HE:

$$S_{HAP} = \frac{(4L_{HAP}+2)MW_{HAP}}{a_{HAP}\rho_{HAP}} \quad [A3]$$

$$a_{HAP} = \frac{[HAP_{HE}]MW_{HAP}L_{HAP}^2}{\rho_{HAP}\sqrt[3]{se_{HAP}}} + \sqrt[3]{se_{HAP}^2}a_{HAP_0}^3 \quad [A4]$$

$$se_{HAP} = se_{HAP_0} + \frac{[HAP_{HO}]MW_{HAP}L_{HAP}^2}{\rho_{HAP}a_{HAP_0}^3} \quad [A5]$$

Detailed equations for diffusion through crystal barrier:

$$d_{barr} = \frac{(100[Ca] + 502[HAP] + 136[MON] + 366[HAP_2]) \times n}{\rho_{barr}S(n-1)} \quad [A6]$$

Detailed equations for exhaustion functions:

$$pH_{sat} = P_2 - \frac{P_2 - P_1}{\left(1 + e^{-\frac{P_3}{F}(CaO_{TOT} - F \times P_4)} \right)} \quad [A7]$$

$$\log(k_{diss}) = B_1 + \frac{1}{F} B_2 X_{CaO} + \log \left(0.001S^{\frac{(1-n)}{n}} \right) \quad [A8]$$

$$F = \frac{1000\rho_{slag}(1-n)}{n} \quad [A9]$$

Highlights

- Presentation of a new model for prediction of phosphorus removal by steel slag filter
- Presentation of an experimental procedure for measurement of slag exhaustion behavior
- Model including equations for slag exhaustion, diffusion into crystal barrier, nucleation and crystal growth
- Validation of model equations with microscopic observations (SEM and TEM) and XRD
- Numerical simulations reproduces slag filter experimental data